A Molecular Mechanics Force Field for NAD^+, NADH, and the Pyrophosphate Groups of Nucleotides

JOSEPH J. PAVELITES[†] **and JIALI GAO**

Chemistry Department, State University of New York at Buffalo, Buffalo, New York 14260-3000

PAUL A. BASH

Center for Mechanistic Biology and Biotechnology, Argonne National Laboratory, Argonne, Illinois 60439

ALEXANDER D. MACKERELL, JR.*

Department of Pharmaceutical Sciences, School of Pharmacy, University of Maryland at Baltimore, Baltimore, Maryland 21201

Received 3 January 1996; accepted 26 April 1996

ABSTRACT

Empirical force field parameters for nicotinamide (NIC^+) and 1,4-dihydronicotinamide (NICH) were developed for use in modeling of the coenzymes nicotinamide adenine dinucleotide (NAD^+) and NAD hydride (NADH). The parametrization follows the methodology used in the development of the CHARMM22 all-hydrogen parameters for proteins, nucleic acids, and lipids. Parametrization of inorganic phosphate for use in adenosine di- and triphosphates (e.g., ADP and ATP) is also presented. While high level *ab initio* data, such as conformational energies, dipole moments, interactions with water, and vibrational frequencies, were adequately reproduced by the developed parameters, strong emphasis was placed on the successful reproduction of experimental geometries and crystal data. Results for molecular dynamics crystal simulations were in good agreement with available crystallographic data.

This article includes Supplementary Material available from the authors upon request or via the Internet at ftp.wiley.com/public/journals/jcc/suppmat/18/239 or http://www.wiley.com/jcc

* Author to whom all correspondence should be addressed. E-mail: alex@mmiris.ab.umd.edu

† Current address: Department of Natural Sciences, University of Houston-Downtown, Houston, TX 77002.

Journal of Computational Chemistry, Vol. 18, No. 2, 221–239 (1997)

CCC 0192-8651 / 97 / 020221-19

Simulations of NAD^+ in the enzyme alcohol dehydrogenase compared quite favorably with experimental geometries and protein matrix interactions.

Introduction

Computer simulations of biomolecular systems, such as proteins and DNA in aqueous solution, offer an opportunity to gain insights into the fundamental properties of these molecules. Despite the tremendous progress in computer speed and algorithms for quantum mechanical methods, current computer technology limits routine *ab initio* and density functional calculations to molecules containing a modest 15–20 nonhydrogen atoms. Consequently, empirical molecular mechanics force fields are typically used in molecular dynamics (MD) and Monte Carlo simulations due to their computational efficiency.[1] However, these potential functions must be rigorously parametrized based on small model compounds to produce realistic results for proteins or other large molecules.

Over the past decade, significant effort has been spent on the development of molecular mechanics force fields, and a number of rigorously tested methods have been described in the literature. The CHARMM22 force field was recently developed for proteins, lipids, and nucleic acids.[2–4] All atoms, including aliphatic hydrogens, are treated explicitly in the CHARMM22 force field. The aim of the CHARMM22 force field is a parameter set that is appropriate for condensed phase simulations of biological molecules, using a simplified potential energy function[5] [see eq. (1) below] to maintain computational efficiency. To assure the highest accuracy of the force field, parameter optimization is based on maximizing the reproduction of goal data for a selected set of compounds. The use of this assumption, however, leads to a loss of transferability of the parameters to other molecules not included in the selected set of test compounds. The present parameter optimization project maintains this philosophy as well as the general methodology used in the development of the CHARMM22 force field.

The coenzymes nicotinamide adenine dinucleotide (NAD^+) and NAD hydride (NADH) shown in Figure 1 hold great biological importance as one of the main redox pairs in the energy producing processes of living cells. The NAD^+/NADH redox pair has a pivotal role in the citric acid cycle, the electron transport system, deamination of amino acids in protein metabolism, the synthesis of acetyl coenzyme A (CoA) from fatty acids, and numerous other biological processes.[6] NAD^+/NADH is mainly synthesized in humans from ingested quantities of niacin or niacinamide, members of the family of B vitamins. Despite the human body's ability to also synthesize limited amounts of NAD^+/NADH from the amino acid tryptophan, a deficiency of niacin in the diet results in the disease pellagra, which can be fatal if left untreated.[7] Since the pioneering work of Lohmann, Myerhof, and Parnas in the 1930s, biochemists have realized the central role that adenosine triphosphate (ATP) plays in energy metabolism.[8] Most fundamental processes of the body consume energy in the form of ATP. In turn, adenosine diphosphate (ADP) or adenosine monophosphate (AMP) is produced with the eventual rephosphorylation to ATP, which is fueled by the processes of catabolism.

The use of MD as a tool in the investigation of NAD^+/NADH containing enzymes such as lactate dehydrogenase or liver alcohol dehydrogenase (ADH)[9] or enzymes that utilize ATP as a substrate or produce ATP, such as ATP synthetase,[6] requires that these molecules be parametrized. In this work, we focus on the parametrization of the NAD^+/NADH redox pair and ATP for use in the molecular dynamics computer program CHARMM.[5] To accomplish this goal, a series of model compounds were selected that represent the functionalities in NAD^+ and NADH. Specifically for NAD^+/NADH, the nicotinamide ring will be emphasized (i.e., nicotinamide, NIC^+ and 1,4-dihydronicotinamide, NICH) (Fig. 1c, 1d), along with methyl diphosphate (Fig. 2) to model inorganic phosphate. These parameters will be combined with the previously derived parameters for adenine and ribose[4] to construct the entire NAD^+/NADH and AMP/ADP/ATP molecules; extensions to compounds such as guanosine triphosphate can also be performed. Our parametrization of these compounds is based on the reproduction of experimental and high level *ab initio* results, including, geometries, conformational energies, vibrational frequencies, and crystal properties.

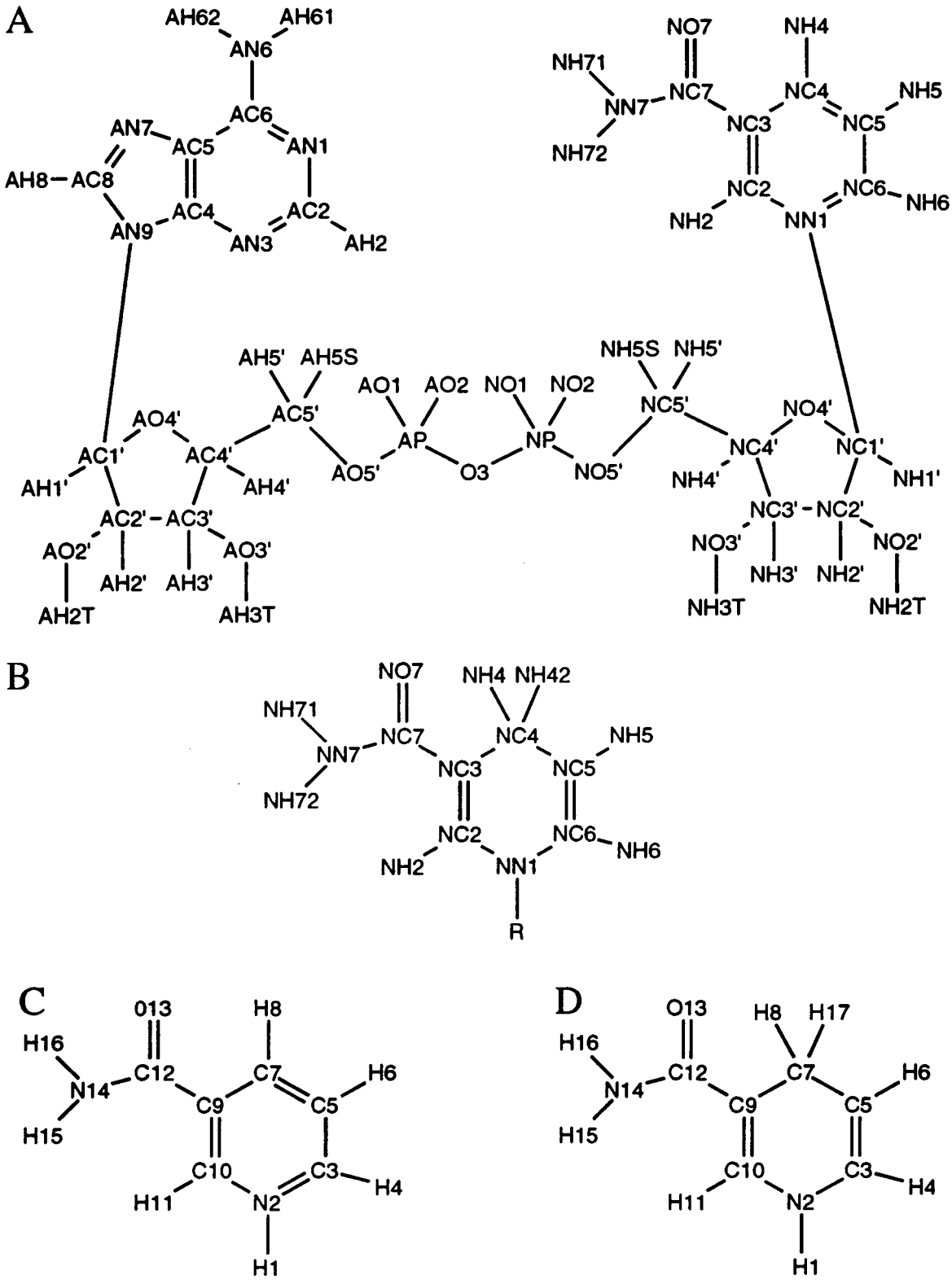

FIGURE 1. (a) Nicotinamide adenine dinucleotide (NAD^+) structure; (b) Nicotinamide adenine dinucleotide hydride (NADH) partial structure. *R* group represents adenine dinucleotide structure as in (a) with NC1′ connected to NN1; (c) nicotinamide; (d) 1,4-dihydronicotinamide. Atomic centers in (a) and (b) are labeled with the Brookhaven Protein Data Bank nomenclature. Labels in (c) and (d) correspond to the atom names used in the text and tables.

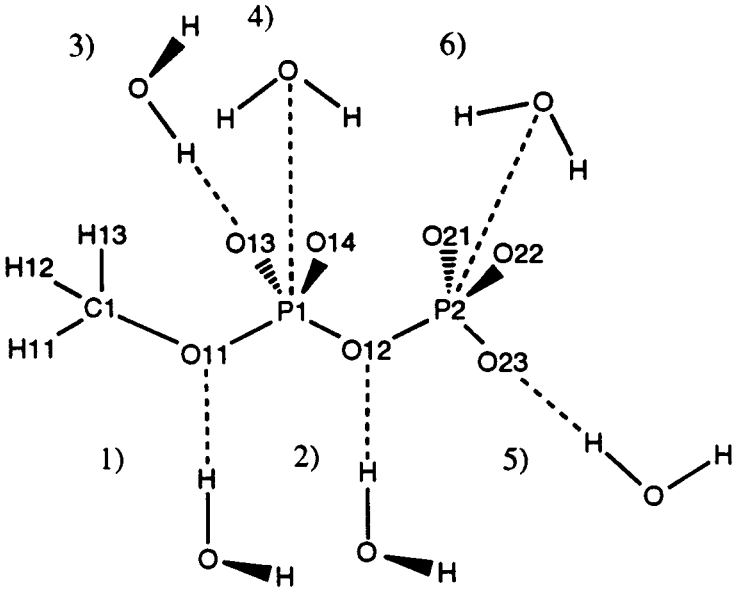

FIGURE 2. Methyl diphosphate interactions with water. (---) Distances being optimized. Atomic centers are labeled with the atom names used in the text and tables.

Parametrization

FORCE FIELD MODEL

The CHARMM energy function[5] is based on a series of functional terms for both internal and nonbonded terms given as follows:

$$V_T = \sum_{\text{bonds}} K_{\text{b}}(b - b_0)^2 + \sum_{\text{angles}} K_\theta(\theta - \theta_0)^2 + \sum_{\text{dihedrals}} K_\phi[1 + \cos(n\phi - \delta)] + \sum_{1,3\text{pairs}} K_{\text{UB}}(S - S_0)^2 + \sum_{\text{improper}} K_w(w - w_0)^2 + \sum_{\text{nonbonded}} \left(\varepsilon_{ij}\left[\left(\frac{R_{\min,ij}}{r_{ij}} \right)^{12} - 2\left(\frac{R_{\min,ij}}{r_{ij}} \right)^{6} \right] + \frac{q_i q_j}{4\pi D r_{ij}} \right). \quad (1)$$

In eq. (1) the first two terms account for bond and angle deformations using a harmonic approximation, where K_{b} is the bond stretching force, constant b_0 is the equilibrium bond distance, and K_θ and θ_0 are the bond angle stretching force constant and the equilibrium bond angle. The third term is a torsion energy based on a cosine function, where K_ϕ is the dihedral force constant, n is the periodicity, and δ is the phase. Dihedral terms may be treated as a Fourier series, if necessary. The fourth term is the Urey–Bradley term, a distance constraint used for the interactions of the first and third atoms of an angle (1, 3 interactions) that are not adequately treated by bond angle bending terms alone. It includes a force constant K_{UB} and 1, 3 equilibrium distance S_0. The fifth term is the improper torsion term that is designed to maintain planarity about planar atoms where K_w is the torsional force constant and w_0 is the equilibrium improper dihedral angle. These terms comprise the internal energy terms.[2]

Nonbonded interactions are described by the familiar Lennard–Jones plus Coulombic terms [last summation in eq. (1)] in which partial atomic charges (q_i) are located on the nuclear centers. Consistent with the CHARMM22 force field, electrostatic and van der Waals (VDW) interactions are enumerated by using a nonbonded exclusion list, which prevents interactions between atoms separated by less than three bonds in the same molecule. Previously, scaling factors ranging from 0.4 to 1.0 were used to reduce the 1–4 interactions. In the present parametrization, the scaling factor (1, 4 factor) is set to unity. The nonbonded exclu-

sion is zero if a pair of atoms are connected by an angle or bond. Lennard–Jones terms ε_{ij} and $R_{\min,ij}$ are determined by combination rules

$$\varepsilon_{ij} = (\varepsilon_i \varepsilon_j)^{1/2} \quad \text{and} \quad R_{\min,ij} = \left(\frac{R_{\min,i} + R_{\min,j}}{2} \right),$$

where r_{ij} is the distance between atoms i and j, and D is the permittivity of a vacuum. Explicit hydrogen bonding terms are not required in the present model.[2,3,4]

ATOM TYPES AND GEOMETRIC PARAMETERS

The new parameters represent an extension of the CHARMM22 nucleic acid parameter set.[4] Initial parameters were extracted directly from those parameters. For the amide of the nicotinamide, parameters were initially transferred from the protein parameter set.[2] Atom types are defined with consideration to introduce a minimal set of new atom types while accurately reproducing experimental and high level *ab initio* results. The atom types employed for NAD^+, NADH, and ATP are summarized in Table I.

Equilibrium bond lengths and angles were adjusted to reproduce the average geometries obtained from X-ray crystallographic data. A search of the Cambridge Structural Database (CSD)[10] provided a wealth of information on molecular geometries from X-ray diffraction studies. The statistical computer package (GSTAT version 5.1)[11] aided in the collection and analysis of this information. Ten crystal structures were found in the CSD for *cis*-NIC^+. In both NIC^+ and NICH structures, the cis configuration describes the orientation of the amide carbonyl oxygen with respect to the nitrogen of the pyridine ring (see Fig. 1), while the trans configuration involves a rotation of the amide by 180°, with the carbonyl oxygen pointing away from the pyridine nitrogen. Because of the reactivity of the reduced form of nicotinamide, no crystal structures were found for NICH. However, the analogous molecule, 1-benzyl-4-[(4-cyanophenyl)hydroxymethyl]-4 hydronicotinamide was used to aid in the definition of the NICH geometry. This molecule differs from NICH by the substitution of the hydrogen of the ring nitrogen by a phenyl group and the substitution of the hydrogen of carbon seven (see Fig. 1d) by the *para*-cyano phenyl alcohol. Two crystal structures for this molecule (CSD code names FIXCUK and FIXDAR)[12] were found. For the phosphate data, six diphosphate and four triphosphate crystals were used for the statistical averaging. Geometric data is presented in Tables S.I–S.IV of the supplemental material.

TABLE I.
Atomic Charges and Atom Type for NIC^+ (Models 1 and 2), NICH, and Methyl Diphosphate.

NIC^+				NICH			Methyl Diphosphate		
		Charge							
Atom	Type	1	2	Atom	Type	Charge	Atom	Type	Charge
H1	HN2	0.44	0.45	HI	HN2	0.42	C1	CN9	−0.17
N2	NN2	−0.55	−0.52	N2	NN2	−0.69	O11	ON2	−0.62
C3	CN3B	0.17	0.16	C3	CN3C	−0.06	P1	P	1.50
H4	HN3B	0.28	0.19	H4	HN3	0.17	O12	ON2	−0.74
C5	CN3	−0.16	−0.10	C5	CN3	−0.18	O13	ON3	−0.82
H6	HN3B	0.22	0.16	H6	HN3	0.14	O14	ON3	−0.82
C7	CN3A	−0.10	−0.05	C7	CN8	−0.28	P2	P2	1.10
H8	HN3B	0.25	0.16	H8	HN7	0.09	022	ON3	−0.90
C9	CN3	−0.16	0.05	H17	HN7	0.09	O23	ON3	−0.90
C10	CN3B	0.17	0.18	C10	CN3C	−0.10	O24	ON3	−0.90
H11	HN3B	0.28	0.16	H11	HN3	0.14	H11	HN7	0.09
C12	CNIA	0.56	0.68	C9	CN3	0.36	H12	HN7	0.09
O13	ON1	−0.40	−0.40	C12	CNIA	0.55	H13	HN7	0.09
N14	NNI	−0.76	−0.82	O13	ON1	−0.51			
H15	HN1	0.38	0.34	N14	NN1	−0.72			
H16	HN1	0.38	0.36	H15	HN1	0.26			
				H16	HN1	0.32			

Model 1 uses the standard CHARMM22 aromatic VDW radii on HN3 type hydrogens. See Results and Discussion section.

FORCE CONSTANTS AND AMIDE DIHEDRAL ROTATION IN NIC AND NICH

Molecular mechanical force constants were obtained following the same methodology as used in the development of the CHARMM22 all-hydrogen parameters for proteins, nucleic acids, and lipids (A. D. Mackerell, Jr. and M. Karplus, manuscript in preparation).[2-4] The objective is to reproduce available experimental and *ab initio* vibrational frequencies by adjusting the appropriate force constants. Geometry optimization and normal mode vibrational frequency calculations were carried out for the cis and trans configurations for NIC^+ and NICH structures at the HF/6−31G(*d*) level, while calculations on the methyl diphosphate monomer were performed at the HF/6−31 + G(*d*) level utilizing the GAUSSIAN 90 program.

The *ab initio* force constants were employed to analyze specific contributions to the harmonic frequencies from internal coordinate motions using the MOLVIB facility in CHARMM.[13] The choice of internal coordinates was based upon the recommendations of Pulay et al.[14] Because vibrational frequencies are systematically overestimated with Hartree−Fock (HF) calculations, a scale factor of 0.9 was used to reduce the *ab initio* results.[15] Force constants in eq. (1) were adjusted to reproduce the vibrational frequencies and to match the vibrational modes as well as reproducing the amide rotational energy surface of NIC^+ and NICH obtained from MP2/6−31G(*d*)//6−31G(*d*) calculations.

Tables S.V−S.VII (supplemental material) show the comparison between the CHARMM calculated vibrational frequencies and the *ab initio* calculated frequencies. *Ab initio* and molecular mechanical rotational energy surfaces for NIC^+ and NICH are presented in Figures S.1 and S.2 of the supplemental material.

PARTIAL ATOMIC CHARGES

Partial atomic charges were determined based on the reproduction of *ab initio* interaction energies and geometries of model compounds as described previously (W. E. Reiher, III and M.

TABLE II.
NIC^+−Water Interactions.

No.	Interaction	*ab initio*			Model 1			Model 2		
		E_{min}	R_{min}	Angle	E_{min}	R_{min}	Angle	E_{min}	R_{min}	Angle
	NIC^+ *trans*									
1	N2—H1 · · OHH	−16.50	1.85		−16.70	1.75		−16.90	1.74	
2	C3—H4 · · OHH	−10.60	2.10		−10.50	2.11		−10.40	2.10	
3	C10—H11 · · OHH	−10.80	2.11		−12.10	2.12		−11.50	2.11	
4	C5—H6 · · OHH	−8.56	2.18		−8.47	2.15		−8.42	2.15	
5	C7—H8 · · OHH	−8.13	2.09		−7.38	2.15		−7.73	2.15	
6	C12—O13 · · HOH1	−5.47	2.02	132°	−5.24	1.83	133°	−5.21	1.82	132°
7	C12—O13 · · HOH2	−3.56	2.06	251°	−3.85	1.86	258°	−3.77	1.87	260°
8	N14—H15 · · OHH	−10.20	2.07		−10.90	1.95		−10.60	1.94	
9	N14—H16 · · OHH	−9.56	1.96		−9.35	1.85		−9.44	1.85	
	NIC^+ *cis*									
1	N2—H1 · · OHH	−16.60	1.84		−16.50	1.75		−16.70	1.73	
2	C3—H4 · · OHH	−10.50	2.11		−10.50	2.11		−10.40	2.11	
3	C10—H11 · · OHH	−9.53	2.04		−9.49	2.12		−9.46	2.12	
4	C5—H6 · · OHH	−8.59	2.19		−8.70	2.15		−8.61	2.15	
5	C7—H8 · · OHH	−9.73	2.20		−10.70	2.17		−10.10	2.15	
6	C12—O13 · · HOH1	−6.33	1.98	135°	−6.44	1.80	136°	−6.14	1.88	135°
7	C12—O13 · · HOH2	−3.52	2.05	252°	−3.45	1.88	259°	−3.39	1.89	261°
8	N14—H15 · · OHH	−10.30	2.10		−8.81	2.34		−10.00	2.00	
9	N14—H16 · · OHH	−9.57	1.96		−9.09	1.86		−9.23	−1.86	

Interaction energies and geometries were determined with only the single, specified water molecule present. E_{min} (energies) in kcal / mol; R_{min} (distances) in Å.

TABLE III.
NICH–Water Interactions.

No.	Interaction	*Ab initio* E_{min}	*Ab initio* R_{min}	*Ab initio* Angle	Empirical E_{min}	Empirical R_{min}	Empirical Angle
			NICH *trans*				
1	N2—H1 · · OHH	−5.72	2.13		−6.00	1.85	
2	C3—H4 · · OHH	−2.16	2.58		−1.71	2.56	
3	C10—H11 · · OHH	−3.03	2.44		−2.71	2.53	
4	C5—H6 · · OHH	−1.23	2.72		−1.04	2.60	
5	C7—H8 · · OHH	−0.18	2.89		−0.30	2.75	
6	C7—H17 · · OHH	0.28	2.65		0.17	2.68	
7	C12—O13 · · HOH	−6.29	2.01	142°	−6.30	1.77	146°
8	C12—O13 · · HOH	−7.33	1.96	242°	−7.56	1.77	253°
9	N14—H15 · · OHH	−5.58	2.15		−5.16	1.98	
10	N14—H16 · · OHH	−4.21	2.11		−4.17	1.92	
			NICH *cis*				
1	N2—H1 · · OHH	−6.12	2.10		−5.74	1.85	
2	C3—H4 · · OHH	−2.41	2.55		−1.68	2.56	
3	C10—H11 · · OHH	−1.21	2.32		−0.41	2.32	
4	C5—H6 · · OHH	−1.40	2.73		−1.23	2.60	
5	C7—H8 · · OHH	−1.18	2.70		−1.77	2.62	
6	C7—H17 · · OHH	−1.51	2.76		−0.96	2.69	
7	C12—O13 · · HOH	−8.93	1.94	141°	−6.56	1.76	148°
8	C12—O13 · · HOH	−9.03	1.94	244°	−7.37	1.80	254°
9	N14—H15 · · OHH	−2.95	2.68		−2.76	2.58	
10	N14—H16 · · OHH	−4.10	2.11		−4.03	1.93	

For NICH the *ab initio* interactions energies are scaled by 1.16 (see text). Interaction energies and geometries were determined with only the single, specified water molecule present. E_{min} (energies) in kcal / mol; R_{min} (distances) in Å.

Karplus, unpublished results).[16–18] In each case, several hydrogen bonded complexes were individually optimized via *ab initio* calculations using the $6{-}31G(d)$ basis set with fixed monomer geometries, and with the present molecular mechanics force field and the TIP3P water model[19] (Tables II–IV). Typically only the hydrogen bond distance and in some cases a single angle are included in the optimization (Figs. 2, 3). The partial atomic charges are adjusted to reproduce the *ab initio*

TABLE IV.
Methyl Diphosphate–Water Interactions.

No.	Interaction	*Ab initio* E_{min}	*Ab initio* R_{min}	Empirical E_{min}	Empirical R_{min}
1	O11 · · HOH	−18.7	1.86	−17.0(1.11)	1.79
2	O12 · · HOH	−16.2	2.31	−17.6(−0.41)	1.89
3	O13 · · HOH	−23.2	1.73	−18.5(2.37)	1.64
4	P1 · · HOH	−20.8	3.64	−19.9(−0.16)	3.51
5	O24 · · HOH	−26.2	1.70	−23.1(3.21)	1.60
6	P2 · · HOH	−23.7	3.63	−26.1(0.48)	3.44

Values in parentheses for the empirical E_{min} are the VDW contribution to the interaction energy.
Interaction energies and geometries were determined with only the single, specified water molecule present. E_{min} (energies) in kcal / mol and R_{min} (distances) in Å.

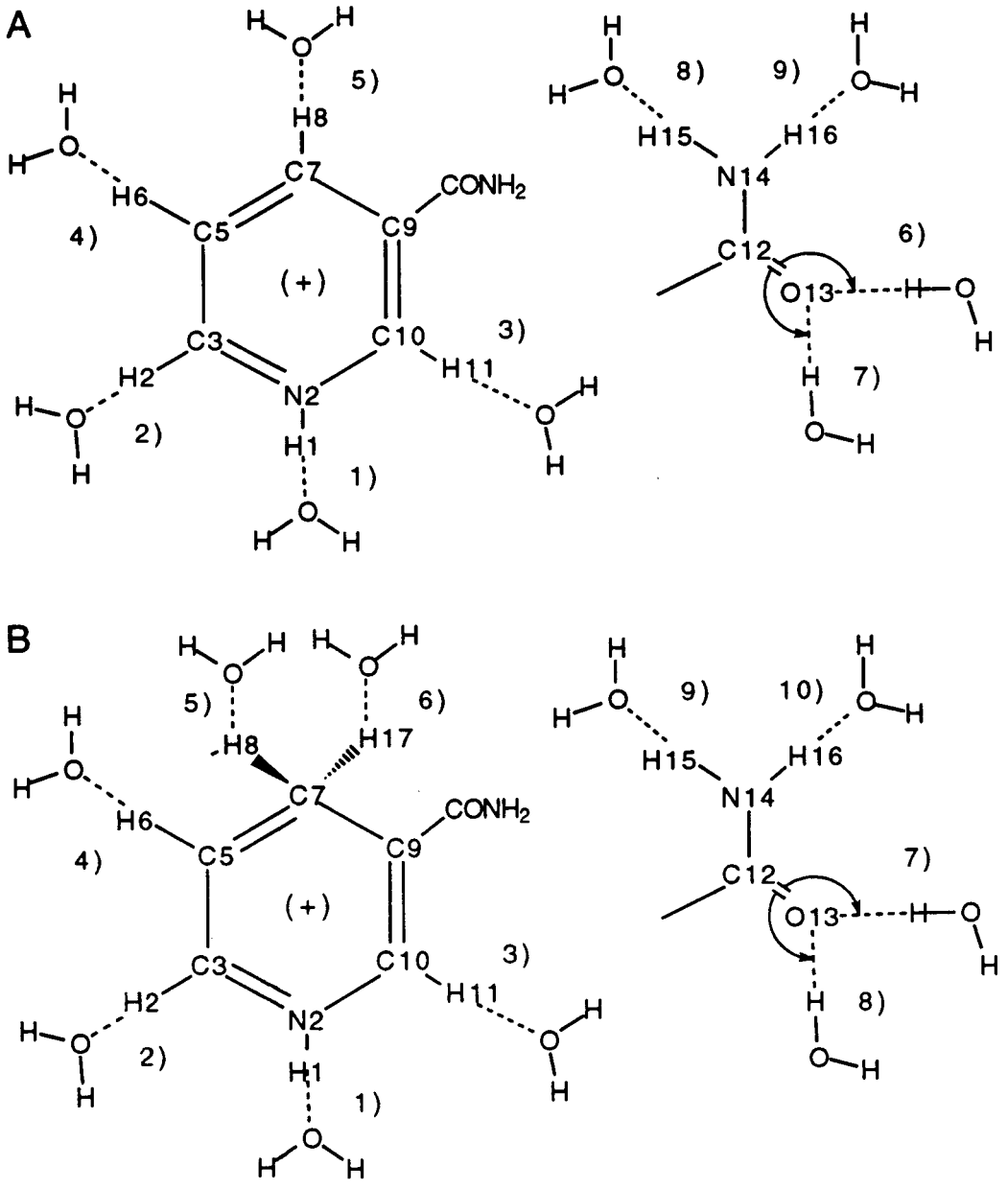

FIGURE 3. (a) NIC^+ and (b) NICH interactions with water. (---) Distances being optimized; angles being optimized are represented by curved arrows.

geometrical and energetic results. In the case of neutral species, the *ab initio* interaction energies are scaled by 1.16,[18] and the distances are offset by -0.1 to -0.2 Å.[17] These scaling procedures were shown to produce empirical force field parameters that yield condensed phase properties, such as heats of vaporization and molecular volumes, in good agreement with the experiment. In addition, the magnitude and direction of the dipole moment based on the empirical charges were checked with respect to the HF/6–31G(*d*) values.

CRYSTAL SIMULATIONS

Crystal simulations allow a rigorous test of empirical force field parameters in the condensed phase. This is due to the detailed intramolecular geometries and intermolecular interactions that may he obtained from small molecule X-ray crystallography. Accordingly, crystal minimizations and simulations were performed as a final test of the presented parameters. In addition, the NAD^+ crystal calculations offered an additional criteria

by which to select from the two nonbonded models developed in this study. A stereodiagram of the NAD^+ asymmetric crystal, including nearest neighbors in the crystal and the unit cell, is shown in Figure 4.

Computational Details

Molecular mechanics calculations were carried out using the program CHARMM.[5] Energy minimizations of the model compounds were performed by applying 200 steps of adopted-basis Newton–Raphson (ABNR) minimization followed by Newton–Raphson minimization to a final gradient of 10^{-6} kcal/mol/Å. All possible interactions were included in the nonbond list. Frequencies were determined using the VIBRAN facility, and analysis of the internal coordinate contributions to the frequencies was carried out with the MOLVIB module.[13] Molecular mechanical calculations of hydrogen bonded complexes for the model compounds used the gas phase minimized structures and the TIP3P water model.[19] Interaction energies between a single water molecule and the model compounds were calculated as a function of distance and in some cases for one angle for idealized hydrogen bonded interactions. Crystal calculations were performed using the CRYSTAL facility in CHARMM.[5, 20] Calculations were performed using a shift truncation for electrostatic interactions and a switch truncation for the VDW interactions; truncation distances are reported in the text. Minimizations were performed by initially fixing all nonhydrogen atoms and minimizing for 50 ABNR minimization steps with the lattice parameters fixed. This was followed by 200 ABNR steps with the lattice parameters fixed followed by 1000 ABNR steps, including the lattice parameters, or until a root means square (rms) gradient of 10^{-6} kcal/mol/Å was achieved. Crystal simulations were performed for 20 ps in the NVT ensemble[21] with a temperature coupling constant of 0.1 ps^{-1}, using the leap-frog integrator with a timestep of 1 fs and the SHAKE algorithm to constrain all covalent bonds involving hydrogen atoms.[22]

Molecular dynamics simulations of ADH[23] in water were performed with stochastic boundary conditions.[24] Details of the simulations will be presented elsewhere (P. Bash, Work in progress). Briefly, the water was thermalized for 40 ps with the protein, NAD^+, and ethoxide substrate fixed after the introduction of solvent following standard procedures. Simulations were performed with the Verlet algorithm using an integration time step of 0.002 ps. SHAKE was used to constrain all covalent bonds involving hydrogens[22] along with a nonbonded truncation scheme where the electrostatics shifted to zero at 12 Å and the VDW interactions were scaled using a switch function between 10 and 12 Å. This was followed by a 80-ps equilibration, allowing all atoms in the system to move. A production simulation of 330 ps was performed from which averages and rms fluctuations were obtained from coordinates saved every 0.2 ps for comparison with the experimental crystal structure.

X-ray crystallographic data were obtained for components of NAD^+, NADH, and ATP from the CSD.[10] Statistical analysis of the geometrical survey data was performed with GSTAT version 5.1.[11]

Ab initio geometry optimizations and vibrational frequency calculations were performed with the Gaussian 90 suite of programs.[25] The contributions of the internal coordinates to the computed vibrational frequencies were analyzed with the MOLVIB facility in CHARMM using the force constants and geometries determined by the *ab initio* calculations. Hydrogen bonded complexes between model compounds and water were studied analogously as in the empirical force field calculations. Again. only partial geometry optimization was carried out for these complexes with fixed monomer geometries.

Results and Discussion

NICOTINAMIDES

Analysis of structural results (Tables S.I and S.II of the supplemental material) show that the empirical bond lengths for the NIC^+ and NICH monomer structures are in good agreement with the average crystal survey data. The NIC^+ model bond lengths have an rms difference of 0.011 Å with respect to the crystal data. This deviation is similar to the statistical error for the majority of the bond lengths determined in the structural survey. The N14–C12 bond length is the worst case for NIC^+, with a 0.030-Å deviation from the experiment. Because 1,4 dihydronicotinamide crystal data is not available, target geometries for the CHARMM NICH model were chosen to be values intermediate to the crystal data of analogous compounds and the *ab initio* data. In general, the bond lengths for NICH fall within the range of the experimental

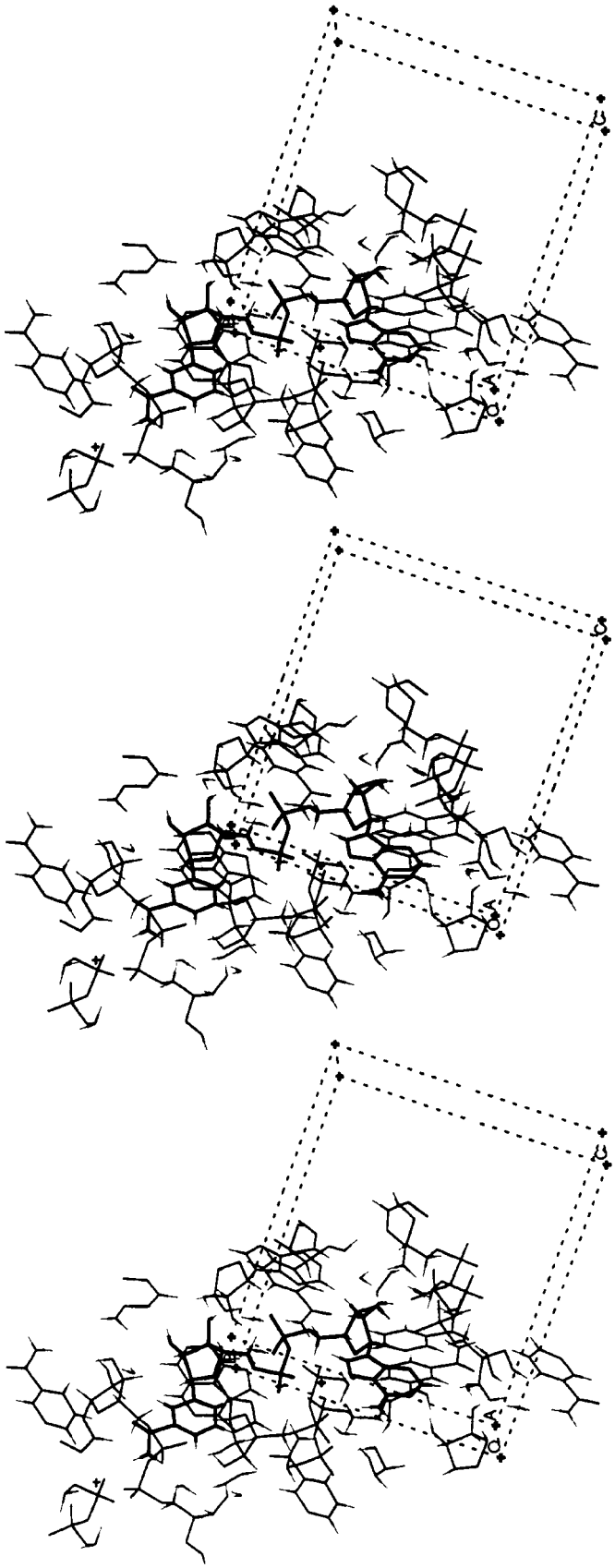

FIGURE 4. Stereodiagram of NAD^+ crystal asymmetric unit (bold lines) including nearest neighbors (thin lines) in the crystal. (···) Unit cell.

and *ab initio* data, with the exception of the slightly overestimated C7–C9 and C9–C12 bond lengths that lie outside their respective ranges by 0.012 and 0.035 Å. Note that the N14–C12 bond length falls within the target range.

Experimental bond angles were reproduced reasonably well for the nicotinamide compounds. Bond angles for the heavy atoms of CHARMM NIC^+ model differ from the crystallographic data with an rms difference of 2.0°. This difference is slightly larger than the error in the survey results. The heavy atom angles of the CHARMM NICH model generally fall within the experimental and computational values, with the largest deviation being the H6–C5–C7 angle, which lies 0.8° below its range.

Limitations in the agreement of empirical geometries and the goal data may be attributed to two items. First, to maintain consistency with the protein amide parameters, only parameters associated with new atom types were optimized. This condition lead to the C12–N14 bond length being too long for both NIC^+ and NICH. Second, identical amide parameters were used for both NIC^+ and NICH. This use of identical amide parameters led to the poor agreement for the C9–C12 bond length in NICH, where that bond is in good agreement for the NIC^+ model. While such limitations could be alleviated by using different atom types for NIC^+ versus NICH, the overall quality of agreement was deemed satisfactory to maintain one set of atom types.

A comparison of dihedrals for NIC^+ show that the minor deviation from planarity for the nicotinamide ring in the crystal structures is well reproduced by the present model. Similar dihedrals are seen in the *ab initio* results, although the ring maintains its planarity. NICH parametrization began with the assumption that the our NICH model would have a planar ring geometry, the belief being that an initially flat but flexible ring would distort due to interactions with its environment. Starting from this planar geometry the ring would have better (i.e., less biased) access to more realistic conformations. However, this concept was abandoned when it was found that vibrational frequencies and the amide rotational energy surface could not be adjusted to adequately reproduce corresponding target data. The amide's sensitivity to conformational change based on environmental factors is necessary and desirable.[26,27] The present NICH model also exhibits the expected ring conformational flexibility that is exhibited in the experimental structures.

Wu and Houk discussed the importance of the conformational features of NIC^+ and NICH in their roles as coenzymes in NAD^+/NADH dependent dehydrogenases.[26,27] The out of plane distortion of the nicotinamide amide may have significant influence on the catalysis and stereochemistry of hydride transfer during its role in enzymatic reactions.[27] Because of this influence, the ability of our empirical parameters for NIC^+ and NICH to faithfully recreate the relative energy difference between the cis and trans conformations as well as the relative energy barrier between the two conformers is of great importance. Wu and Houk found that the cis conformation of NIC^+ is 1 kcal/mol more stable than the *trans*-NIC^+ conformer with a 4 kcal/mol energy barrier upon rotation of the amide group from cis to trans. Wu and Houk, based on HF/6–31*G*(*d*) and MP2/6–31*G*(*d*)//6–31*G*(*d*) calculations for NICH, estimate the *cis*-NICH to be more stable than the trans NICH by 1.4 kcal/mol and exhibit a rotational energy barrier of 7.4 kcal/mol for the amide. Our *ab initio* calculations at the HF/ 6–31*G*(*d*) and MP2/6–31*G*(*d*)//6–31*G*(*d*)levels give values of 1.5 and 1.4 kcal/mol, respectively, for the *cis*- and *trans*-NIC^+ energy difference (Fig. S.1 of the supplemental material). The rotational barrier for the *cis*-NIC^+ to *trans*-NIC^+ conformers was found to be 5.3 and 3.6 kcal/mol, at those two theoretical levels, respectively. For the *cis*- and *trans*-NICH energy difference, our *ab initio* calculations at the HF/6–31*G*(*d*) and MP2/6–31*G*(*d*)//6–31*G*(*d*) levels gave values of 1.8 and 1.2 kcal/mol, respectively (Fig. S.2 of the supplemental material). The cis to trans rotational barrier for NICH for the HF/6–31*G*(*d*) and MP2/6–31*G*(*d*)//6–31*G*(*d*) calculations are 7.8 and 7.2 kcal/mol.

The cis conformer for the empirical NIC^+ model is 1.4 kcal/mol lower in energy than the trans conformer, and the cis to trans energy harrier is 4.1 kcal/mol (see Fig. S.1 of the supplemental material). The amide rotational surface for the empirical NIC^+ model reproduces the MP2/6–31(*d*)// 6–31*G*(*d*) energy surface quite well. The shallow minimum at 20° and the small barrier height at 0° in our model is a small exception. However, this is in good agreement with Wu and Houk's[26,27] work that found that the potential energy surface around this region was quite flat and the out of plane distortions had energetic consequences that were quite small.

The rotational energy surface for the NICH model is in good agreement with the results of the *ab initio* calculations (see Fig. S.2 of the supplemen-

tal material). The cis conformer of NICH is more stable than the trans conformer by 1.4 kcal/mol and has a rotational energy barrier for the amide of 8.2 kcal/mol. The trans minima for our NICH model is within 10° of the HF/6−31G(*d*) findings, while the cis minima differs from the HF/6−31G(*d*) calculations by less than 5°. The rotational energy barrier is 1.0 kcal/mol more than the MP2/ 6−31(*d*)// 6−31G(*d*) barrier and 0.4 kcal more than the HF/ 6−31G(*d*) barrier. Such a difference will have only a negligible effect during the sampling that occurs in MD simulations at room temperature.

The internal coordinate contributions to the normal modes of vibration for the NIC^+ model are in good agreement with the target HF/6−31G(*d*) frequency calculations (see Table S.V of the supplemental material). The rms difference between the scaled *ab initio* and empirical frequencies was 119 cm^{-1}, which corresponds to an average percent difference of 6.7%. The important low frequency modes tAMIDE, wAMIDE, and dAMIDE, which are the twisting, wagging, and angle deformations associated with the amide, are in excellent agreement with the *ab initio* modes. This is particularly important for the proper representation of the amide rotational surface. For the lowest 19 modes the rms difference and average percent difference were 44 cm^{-1} and 7.0%. In the case of NICH the overall rms difference was 61 cm^{-1}, corresponding to an average percent difference of 7.9%. The larger average percent difference as compared to NIC^+ is associated with the low frequency modes, although they are in satisfactory agreement with the HF/6−31G(*d*) frequency calculations (see Table S.VI of the supplemental material). Modes associated with the amine vibrations (i.e., tNH_2, wNH_2, $scNH_2$, etc.) are generally too low in the empirical model. This is attributable to the use of existing amide parameters. Efforts to improve the quality of the NICH vibrations via incorporation of a new atom type for the carbonyl carbon were unsuccessful. Out of plane vibrations are particularly important to the floppier NICH ring, and the dihedral and angle deformations tRING and dRING are in satisfactory agreement with the *ab initio* vibrational data. It should be noted that some of the assignments associated with modes greater than 1000 cm^{-1} were not in ideal agreement with the *ab initio* data. Attempts to improve this agreement were unsuccessful. Overall, the agreement with the HF/6−31G(*d*) frequency calculations indicates that the force constants are reliable for both the NIC^+ and NICH force fields.

The variation of angles C10−C9−C12, C7−C9−C12, and C9−C12−N14 as a function of the amide rotation in NIC^+ and the variation of angles O13−C12−C9, C7−C9−C12, and C9−C12−N14 as a function of the amide rotation in NICH for the molecular mechanical and *ab initio* calculations are shown in Figures S.3 and S.4 (supplemental material), respectively. The ability of the force field to reproduce geometric changes for rotation surfaces offers an additional test of the internal force field and the balance between the internal and external portions of the force field. Our NIC^+ force field reproduces the *ab initio* angle variations well. The offset of the *ab initio* and empirical values was expected due to the use of the crystal survey data for the optimization of the NIC^+ geometry. The NICH results, although not as good as the NIC^+, are reasonable, with the largest differences occurring in the high energy regions of the surface that will not be significantly populated during MD simulations. The C7−C9−C12 angle variation shows a break at 90°; this is associated with a change in the ring pucker. Further *ab initio* calculations are needed to better assess the overall fluctuation of the C7−C9−C12 angle. Both empirical models reproduce the *ab initio* trends and are a good indication of the quality of the parameters for modeling geometric changes associated with the rotation of the amide. As stated above efforts were made to improve the agreement of the empirical and *ab initio* geometry and vibrational results for NICH. Addition of a new atom type for the carbonyl carbon did not lead to significant improvement. While the present parameter set yields reasonable results concerning the overall geometry and the rotation of the amide group, it is clear that additional studies on the conformational properties of reduced nicotinamide are warranted.

Partial atomic charges were based on reproducing *ab initio* determined minimum interaction energies and geometries for individual water molecules interacting with a variety of sites around both NIC^+ and NICH. To insure that both the cis and trans forms of both species were adequately treated by the optimized charges, they were each studied explicitly. Presented in Tables II and III are comparisons of the *ab initio* and empirical interaction energies for NIC^+ and NICH with water (see Fig. 3), respectively. For NIC^+ two models are included. Model 1 used the standard aromatic hydrogen ($e_\varepsilon = -0.022$, $R_{min} = 1.32$) and model 2

used a hydrogen that is intermediate to the aromatic and polar hydrogens ($e_\varepsilon = -0.046$, $R_{min} = 0.90$). The intermediate hydrogen was also used in the parametrization of histidine for the CHARMM all atom protein parameters.[2] For NIC^+ it may be seen that both models satisfactorily reproduce the *ab initio* data. The minimum interaction distances are slightly smaller with model 2 due to the use of a small hydrogen VDW radius. Analysis of the interaction energies shows some improvement with model 2 for several of the interactions, including the *trans* C10−H11, *cis* C7−H8, and *cis* N14−H15 interactions. The improvement in the *cis* N14−H15 interaction is due to decreased VDW repulsion from the H11 atom. Based on the improvement in these interaction energies, along with the crystal simulation results (see below), model 2 was selected to represent the nonbonded parameters for NIC^+. The interaction energies for NICH are generally less favorable, and the distances are longer than those in NIC^+, as expected due to the neutral charge of the system. The empirical interaction energies are in satisfactory agreement with the *ab initio* data; however, some differences are evident. For the cis configuration the C7−H8 empirical interaction energy is less favorable than the C7−H17 value. This trend is opposite of that predicted by the *ab initio* calculations. This discrepancy is due to small changes in the internal geometry of the reduced nicotinamide such that the small changes in the relative orientation of the carbonyl oxygen and the C7 atom lead to changes in the interaction energies. This relationship also leads to the differences between the *ab initio* and empirical dipole moment components.

Dipole moments and orientations are included in Table S.VIII (supplemental material). In all cases the dipole moment from the empirical charges is smaller than that from the *ab initio* HF/6−31(d) level of theory. In small, nonaromatic molecules it is generally expected that the empirical dipole moment should be larger than the HF/6−31(d) values, due to the requirement that polarization be included in the parameters using a mean field approximation. An example of this is the TIP3P water model.[19] Dipole moments for the CHARMM22 nucleic acid bases are smaller than the 3−21G(d)//6−31G(d) values for Gua, Thy, and Ura,[4] suggesting that a larger empirical dipole moment may not be required for aromatic systems. Further work is required to clarify this point. Analysis of the X, Y, and Z components of the dipole moments show that they generally reproduce the *ab initio* values. The largest discrepancies tend to occur with the Z component, which may be related to differences in the out of plane empirical and *ab initio* optimized geometries. The agreement of the empirical and *ab initio* components is additional evidence of the quality of the overall empirical charge distributions.

METHYL DIPHOSPHATE

Methyl diphosphate parameters produce good agreement with the results from the crystal structure survey analysis for the internal geometries (see Table S.III of the supplemental material). The overall rms differences are 0.018 and 0.033 Å for the bonds and 5.0° and 4.1° for the angles with respect to the average values for diphosphate and triphosphate from the CSD survey. During the parameter optimization, efforts were made to obtain values intermediate to the diphosphate and triphosphate survey values. This is a desirable feature for parameters that will be used for both ADP and ATP. With respect to the bonds, the only exception is bond r1, the C1−O1 bond length, which is shorter than both the di- and triphosphate values. The parameter associated with this bond was previously optimized based on dimethylphosphate[4] and was not optimized as part of the present study. Considering the standard deviation of the values from the crystal survey it was deemed unnecessary to introduce a new atom type to improve the quality of the empirical model. Comparison of the empirical and crystal survey angles in Table S.III (supplemental material) again shows the empirical values to generally fall between the di- and triphosphate crystal ranges, although several exceptions do occur. Angles a2 and a5, representing the O12−P1−O11 and P2−O12−P1 terms, are both too large. Attempts were made to improve the agreement; however, it was found that this leads to significant changes in the rotational energy surface for methyl diphosphate (see below). With the P2−O12−P1 angle the optimized parameters yield a value intermediate to the CSD and *ab initio* data. Other discrepancies occur with the angles involving the anionic oxygens (e.g., O13, O14, O21, O22, and O23). However, the averaged bond angles (a3a4, a678 and a368) are within the error range of the structural survey values as judged by the standard deviations.

Optimization of the force constants associated with the methyl diphosphate bond, angle, and Urey−Bradley terms was primarily based on reproducing the scaled HF/6−31 + $G(d)$ vibrational spectra. The empirical and *ab initio* spectra are

compared in Table S.VII (supplemental material). The overall rms difference is 44 cm^{-1} and the average percent difference is 5.9%. In the low frequency region, the agreement is excellent with respect to the frequencies and the assignments. This includes torsional motions about the phosphodiester linkage, the methyl rotation, and the P−O−P angle deformation. To obtain this level of agreement, it was necessary to introduce a Urey−Bradley term on the P−ON2−P2 angle, which uses a negative force constant (see Table S.XVI of the supplemental material). This term was also essential for reproducing the methyl diphosphate rotational surface (see below). These low frequency modes dominate the large-scale motions of the diphosphate that can occur during MD simulations. The agreement is also good for the frequencies between approximately 300 and 1000 cm^{-1} (modes 8−20), which are dominated by distortions of the individual phosphates. Accord between our force field and *ab initio* results is also satisfactory for higher modes dominated by stretching terms and distortions of the methyl group. The overall agreement of the empirical and *ab initio* vibrational spectra indicates that the present force field can accurately model the distortions of methyl diphosphate, which will occur in dynamics simulations.

Minimum interactions energies and distances between water and methyl diphosphate (Fig. 2) is depicted in Table IV from the *ab initio* and empirical calculations. Due to the charged nature of the solute, the HF/6−31G(*d*) minimum interaction energies are used directly as the target data. Comparison of the *ab initio* and empirical data shows that the empirical charges adequately reproduce the hydrogen bonding interactions, although the ordering is not ideal. Included in Table IV are the VDW contributions to the empirical interaction energies. As may be seen these contributions are significant for some interactions, being large enough to influence the ordering of the interactions. Similar results were obtained with dianionic methyl phosphate.[4] The quality of the interactions with water indicate the present charge distribution to be satisfactory and is supported by the quality of the parameters in reproducing nonbonded interactions in crystal simulations (see below and ref. 4).

Verification of the pyrophosphate parameters was performed by comparing the pyrophosphate 2-dimensional (2-D) surface with both *ab initio* and experimental crystal data. Figure 5 presents the O12−P1−O11−C1 versus P2−O12−P1−O11 adiabatic surface for pyrophosphate from the present parameter set. Included in the figure are conformations obtained from a search of the CSD for molecules containing C−O−P−O−P fragments. These include diphosphates, triphosphates, and other pyrophosphates, such as that occurring in NAD^+. Comparison of the energy surface and the crystal conformations show the majority of the experimental points to lie within low energy regions of the surface. This supports the validity of the present parameter set with respect to the conformational properties of pyrophosphate. Some crystal structures, however, occur in high energy regions of the surface. These structures are generally of a lower resolution or contain additional atoms attached to the phosphate groups. For example, the point at (−125°, 132°) corresponds to the NAD^+ crystal structure in which the phosphate is linked at both ends to ribose moieties. In simulations of the NAD^+ crystal the corresponding dihedrals were adequately reproduced (see below). The point at (−145°, 68°) corresponds to diphosphate bound at both ends to naphthyl rings (NAPYPX1O); both the covalent linkage to aromatic moieties and conformational constraints are expected to alter the conformational properties of the system. Other examples include the points at (−103°, −178°) (NACYTD) and (175°, −124°)

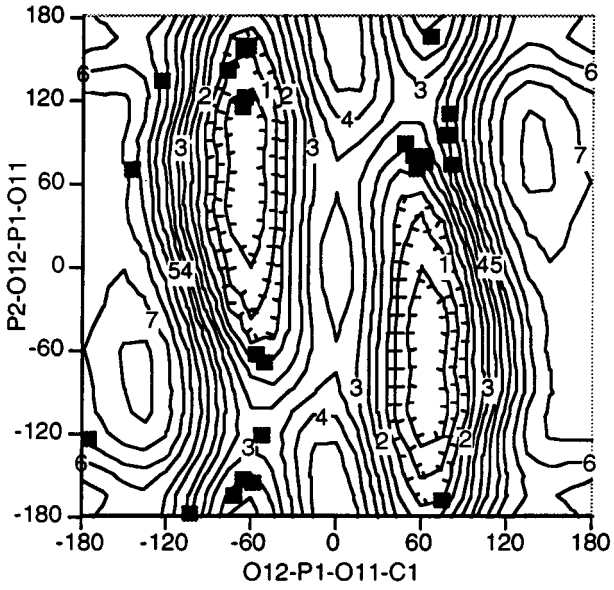

FIGURE 5. Methyl diphosphate 2-D adiabatic energy surface for dihedral angle O12−P1−O11−C1 versus dihedral angle P2−O12−P1−O11. Energies (kcal / mol) were offset such that the minimum energy is equivalent to zero. Contour lines represent 0.5 kcal / mol.

(CDPCHM) in which the termini of the diphosphate are covalently linked to an amine and a trimethylamine respectively. In addition it is expected that the condensed phase environment of the crystals will influence the experimental conformations.

As an additional test of the methyl diphosphate 2-D surface, *ab initio* calculations were performed to sample the P2–O12–P1–O11 dimension. In these calculations the P2–O12–P1–O11 dihedral was constrained while the remainder of the molecule was allowed to relax. Calculations were performed at the HF/6–31 + $G(\delta)$ level of theory. Shown in Table V are the *ab initio* and empirical results. Note that data between 60° and 240° is omitted; initial attempts to obtain *ab initio* optimized geometries in this region were not successful. Due to limitations in computational resources further attempts were not made. Comparisons of the relative energies show the empirical results to satisfactorily reproduce the *ab initio* data. The broad minima between 240° and 360° is present although the empirical surface is energetically ''flatter'' and there is a small local maximum in the vicinity of 285°. Also included in Table V are the O12-P1–O11–C1 and O23–P2–O12–P1 dihedrals as a function of the P2–O12–P1–O11 value. In both cases the *ab initio* trends are generally reproduced by the empirical force field. For the O12–P1–O11–C1 term the change in the empirical data is smaller than the *ab initio* values. For the O23–P2–O12–P1 surface, the empirical force field yields somewhat larger variations than the *ab initio* data. Overall these results support the accuracy of the empirical force field in adequately representing the conformational properties of methyl diphosphate.

NAD^+ CRYSTAL SIMULATIONS

NAD^+ was crystallized in the presence of lithium and two water molecules with the structure resolved to an *R* factor of 0.10 based on data collected to a resolution of 1.09 Å (CSD code NADLIH10).[28] The system crystallizes in an orthorhombic P_{212121} space group with four NAD^+ molecules per unit cell. Calculations were performed on the asymmetric unit, comprising one NAD^+ molecule. Presented in Table S.IX (supplemental material) are the final unit cell parameters and energies from the minimizations using models 1 and 2 with a preliminary model for the diphosphate. In both cases increasing the truncation distance leads to changes in the unit cell parameters and the total energy of the system becoming more favorable. Significant changes also occur in the lattice energies. At the longer distances changes in the values become smaller, indicating that the systems are approaching convergence. At the two longest cutoffs the values may be assumed to be reasonably converged. Therefore, simulations were performed using the 22–21–19 scheme where 22 Å is the cutoff distance for the nonbond interaction list, 21 Å is the cutoff distance for shifted electrostatic interactions and the switched VDW interactions, and 19 Å is the distance where the VDW switching (or cubic smoothing) function is turned on.

TABLE V.
Relative Energies and Ester Dihedral Angles from *ab initio* (AI) and Empirical (Emp) Calculations for Methyldiphosphate as a Function of P2–O12–PI–O11 Dihedral Angle.

	Energy		O12–P1–O11–C1		O23–P2–O12–P1	
P2–O12–P1–O11	AI	Emp	AI	Emp	AI	Emp
0.00	0.20	0.50	65.6	60.4	−51.5	−66.8
60.00	0.77	1.58	50.0	52.5	−93.4	−111.6
240.00	0.95	0.25	60.0	65.1	75.1	65.1
255.00	0.44	0.02	62.7	63.7	61.1	52.6
270.00	0.11	0.06	66.4	63.6	46.8	35.3
287.40[a]	0.00	0.15	70.3	63.4	28.7	9.8
300.00	0.03	0.06	71.6	63.3	14.3	−18.1
315.00	0.10	0.00	71.5	63.9	−4.0	−34.4
345.00	0.18	0.29	68.2	61.8	−37.9	−56.8
360.00	0.20	0.50	65.6	60.4	−51.5	−66.8

Energies are given in kcal / mol and angles given in degrees.
[a] Empirical data correspond to 285°.

Comparison of the model 1 and 2 parameters was performed based on the overall unit cell parameters and specific nonbonded interactions involving the nicotinamide ring. For model 1, it may be seen that unit cell dimensions A and C expand, while B contracts. For model 2, on the other hand, only C expands while A and B both contract. Changes in the nonbonded distances are presented in Table S.X (supplemental material). Comparison of the calculated interaction distances indicates that the model 2 values are generally shorter than the model 1 results. Average differences are 0.08 and 0.03 Å for models 1 and 2, respectively, showing model 2 to be in better agreement with the experiment as compared to model 1. This is also evident in the dynamics results where average differences of 0.33 and 0.15 Å were obtained for models 1 and 2, respectively. Accordingly, model 2 was selected for the nonbonded parameters for the oxidized form of the nicotinamide ring.

Final calculations on the NAD^+ crystal were done using the model 2 parameters with the final diphosphate parameters. The change in the phosphate parameters had only a minor effect on the crystal calculations. With the new parameters, the minimizations with the 22−21−19 truncation scheme yielded optimized lattice parameters of $A = 9.937$, $B = 15.418$, and $C = 18.175$ Å. These correspond to changes of -1.3, -2.7, and 2.0% in each unit cell parameter in comparison with crystal data and indicate that the overall balance of the parameters is adequate. Inspecting the NAD^+ crystal in Figure 5 reveals that the long axis of the molecule lies approximately along the B axis of the crystal, while both the A and C axis are perpendicular to the long axis. Thus, the contraction of the B axis in the minimization indicates that the overall conformation of the molecule is maintained. Stacking of the adenine and nicotinamide bases will contribute to changes in both the A and C axis. The small change in these terms suggests that these interactions are reasonably treated.

Additional details from the calculations using the model 2 parameters are presented in Tables S.XI and S.XII (supplemental material) for the dihedral angles and the interaction distances, respectively. Root mean square differences between the average values from the experiment and the dynamics simulation for the dihedrals was 12.7°. Clearly, the calculated internal geometries are in agreement with the experiment. The largest deviations are about 30°, while the majority of the differences are less than 10°. This level of agreement shows that no significant changes in the internal conformation of the molecules occurred during the minimizations or simulations. Of specific interest are the differences in the NC2−NC3−NC7−NO7 and NC2−NC3−NC7−NN7 dihedrals, which describe the conformation of the nicotinamide amide group. As may be seen both dihedrals increase in the calculations, corresponding to a slight rotation of the amide with respect to the ring. Although these changes are on the same order as the rms fluctuations in the solid state along with relatively large B factors for the amide O and N atoms, the nature of the motion was investigated in more detail. Visual analysis showed the change to involve a shift in the side of the ring adjacent to the amide and the carbonyl group, while the position of the amide group was relatively unchanged. These changes appear to be related to the nonbonded interactions in which the amide participates (see below; Fig. 4), leading to the high flexibility of the amide group as evidenced by both the calculations and experiment. Additional optimization of the amide parameters was not deemed necessary due to the flexibility observed in the crystal and due to results from the ADH simulations (see below).

The computed interaction distances in Table S.XII (supplemental material) are in accord with the experimental values. The overall rms difference is 0.27 Å for the minimizations and 0.26 Å for the simulation. The small improvement in the value upon adding kinetic energy to the system is consistent with the results for the dihedral angles (see Table S.XI of the supplemental material) and emphasizes the importance of treating crystals at the finite temperature at which the experimental data was obtained. The magnitude of the rms differences is dominated by several interactions where differences of 0.4 Å or more occurred. A number of these interactions involve the NO1 and NO2 atoms of the diphosphate bridge. These changes often involve interactions of those atoms with another hydrogen bond acceptor (e.g., AN7) or a carbon atom. Furthermore, a number of interactions involving these atoms, as well as the AO1 and AO2 atoms, are well modeled by the present force field. Note that the phosphate VDW parameters were not subjected to optimization in the present study to maintain consistency with the CHARMM22 nucleic acid and lipid parameters. The crystal simulation results, however, along with independently reported studies[29] suggest that further investigation into the phosphate nonbonded parameters is warranted. For interactions involv-

ing hydrogen bonds (e.g., NAD1 AO2′–WATX OH2 and NAD1 AN6–C003 NO2′) the agreement with the crystal structure is generally much better than the overall rms differences for all interactions.

Interactions involving the amide group oxygen and nitrogen atoms aid in understanding the changes in the conformation shown in Table S.XI (supplemental material). Analysis of Table S.XII (supplemental material) shows that those two atoms (NO7 and NN7) are only involved in four interactions, based on the 3.5-Å cutoff criteria (see Fig. 5). One of these interactions is with a carbon (NO7–AC8), two are with the same water molecule (CO20–OH2), and the fourth is with an anionic phosphate oxygen atom (NO2–NN7). The interaction with the carbon may be considered relatively weak, while shifts in the position of the water molecule involved in the interactions will lead to changes in that region of the molecule. The *B* factor of that water from the crystallographic study is relatively large, consistent with the large values for the amide O and N atoms, further suggesting that this region of the molecule is poorly resolved in the experimental study. In addition, the NC4 carbon involved in the oxidation/reduction process interacts with the same water molecule, possibly contributing to the shift in the nicotinamide ring. The final interaction with the anionic oxygen is satisfactorily reproduced by the force field.

Of note are the interactions involving the lithium ion.[30] Interactions with ions are generally thought to be poorly modeled by potential energy functions such as that in CHARMM due to the lack of an explicit term for electronic polarizability. Analysis of the results in Table S.XII (supplemental material), however, show the present force field to reasonably model the interactions observed in the crystal. The general increase in the distances in the MD simulation does indicate that a shift of the environment around the ion occurred.

ADH SIMULATION

Because the present parameters were designed to be used in biomolecular simulations, it is important to perform a test MD simulation on a protein containing NAD^+. For this study the enzyme ADH was selected. The crystal structure used was the ternary complex (ethanol) of ADH resolved[23] to an *R* factor of 18.3.

Analysis of the time-averaged structure showed an rms difference of 0.85 Å for all protein nonhydrogen atoms and 0.74 Å for the NAD nonhydrogen atoms with respect to the crystal structure. Because of the low resolution of the crystal (2.1 Å), these changes may be considered to be within the accuracy of the structure. Comparison of the experimental and calculated internal dihedrals of NAD^+ are shown in Table S.XIII (supplemental material). The overall rms difference between the experiment and the average values from the simulation was 43.3°. For the majority of dihedrals, however, the differences between the calculated and experimental values are less than 10°. Exclusion of four dihedrals that changed by over 100° yields an rms difference of 14.2°. These dihedrals involve part of the diphosphate connecting the two sugar moieties of NAD^+. The changes that occur do so in a correlated fashion such that the overall structural differences are minimal as evidenced by the rms difference of the atomic positions of 0.74 Å. Possibly also contributing to the change in these dihedrals is the exposure of the associated atoms to solvent in the crystal structure (see below). Notably, the corresponding dihedrals in the NAD^+ crystal calculations (see Table S.XI of the supplemental material) were in good agreement with the experiment. Concerning the nicotinamide ring it may be seen that the agreement with the experiment is excellent, including those for the amide. Thus, the assertion that the changes in the amide dihedrals in the NAD^+ crystal simulations are associated with the flexibility of the amide appears to be reasonable (see above). Combined, the NAD^+ crystal and ADH calculations indicate that the present force field can accurately model the internal conformations of NAD^+.

Results from the ADH simulation were also analyzed for the interactions between NAD^+ and the surrounding environment. Those results are presented in Table S.XIV (supplemental material). As with the NAD^+ crystal, the majority of experimental and calculated interatomic distances are in good agreement. The average and rms differences are 1.21 and 3.40 Å, respectively. However, a number of interactions with water have changes of greater than 1.0 Å, and a large rms difference also occurred between the AC5′ atom of NAD^+ and a peptide nitrogen on the protein, associated with some of the changes in the dihedrals discussed above. Removal of the interactions with an rms difference greater than 1.0 Å from the determination of the average and rms differences yields values of 0.20 and 0.28 Å, respectively, indicating the overall agreement to be satisfactory. It should be noted that a number of the large differences in the interatomic distances involving water molecules occur with the diphosphate and adenine

sugar atoms of NAD^+. These larger differences, which are due to the exchange of the initially bound waters with the bulk solvent, may also contribute to the large change in the conformation of these moieties as discussed above. It is of interest to examine the interactions of the nicotinarnide ring with the environment. The amide moiety participates in interactions with backbone atoms; all of these interactions are reproduced in the simulation. Interactions at the reduction site, the NC4 atom, are also well reproduced in the simulations. These include interactions involving the carboxylate group of an aspartate and the ethoxide substrate. Further, a number of interactions involving the diphosphate with the solvent and with the protein matrix are accurately reproduced. Finally, the interaction between the catalytic zinc[31] and the NC5 atom of the nicotinamide moiety of NAD^+ is satisfactorily reproduced in the calculation, consistent with the lithium–NAD^+ interactions presented above. These results further support the nonbonded model for the nicotinamide and the diphosphate developed in the present study.

Conclusion

Tables S.XV–S.XIX (supplemental material) present empirical force field parameters for NIC^+ and NICH that were developed for use in modeling of the coenzymes NAD^+ and NADH. Parametrization of inorganic phosphate parameters for use in nucleotide di- and triphosphates (e.g., ADP and ATP) are also presented. The parametrization follows the methodology used in the development of the CHARMM22 all-hydrogen parameters for proteins, nucleic acids, and lipids; the current parameters are consistent with previous CHARMM parameters. Previously developed parameters used in this study are published elsewhere.[4, 30, 31] High level *ab initio* data, such as conformational energies, dipole moments, interactions with water, and vibrational frequencies, were adequately reproduced by the developed parameters. In addition, strong emphasis was placed on the successful reproduction of experimental geometries and crystal data. Results for MD crystal simulations are in good agreement with available crystallographic data while a simulation of NAD^+ in the enzyme ADH compares quite favorably with experimental geometries and protein matrix interactions. Faithful reproduction of *ab initio* and experimental data make these new parameters a useful addition to the CHARMM22 parameter set and will allow application of MD techniques to a larger number of biochemical systems.

Acknowledgments

A. D. M. would like to thank NCI's Frederick Biomedical Supercomputing Center for computer time and the Mildred Mindell Cancer Foundation for financial support. This work was supported in part by the National Institutes of Health (J. G.). J. J. P. would like to thank Dr. Harry F. King and Dr. Thomas Furlani for inciteful discussions.

Supplementary Material

Nineteen tables and four figures are included in the Supplementary Material (see footnote on page 221).

References

1. (a) J. A. MaCammon and S. C. Harvey, *Dynamics of Proteins and Nucleic Acids*, Cambridge University Press, New York, 1987; (b) C. L. Brooks, M. Karplus, and B. M. Pettitt, *Proteins: A Theoretical Perspective of Dynamics, Structure, and Thermodynamics*, Vol. LXXI, *Wiley Series on Advances in Chemical Physics*, I. Prigognine and S. Rice, Eds., Wiley, New York, 1988.
2. A. D. MacKerell, Jr., D. Bashford, M. Bellott, R. L. Dunbrack, Jr., M. J. Field, S. Fischer, J. Cao, H. Guo, S. Ha, D. Joseph, L. Kuchnir, K. Kuczera, F. T. K. Lau, C. Mattos, S. Michnick, T. Ngo, D. T. Nguyen, B. Prodhom, B. Roux, M. Schlenkrich, J. C. Smith, R. Stote, J. Straub, J. Wiorkiewicz–Kuczera, and M. Karplus, *FASEB J.*, **6**, A143 (1992).
3. M. Schlenkrich, J. Brickmann. A. D. MacKerell, Jr., and M. Karplus, In *Biological Membranes: A Microscopic View from Computation and Experiment*, K. M. Merz, Jr. and Benoit Roux, Eds., Birkhauser, Boston, 1996.
4. A. D. MacKerell, Jr., J. Wiorkiewicz, and M. Karplus, *J. Am. Chem. Soc.*, **117**, 11946 (1995).
5. B. R. Brooks, R. E. Bruccoleri, B. D. Olafson, D. J. States, S. Swaminathan, and M. Karplus, *J. Comput. Chem.*, **4**, 187 (1983).
6. B. Alberts, D. Bray, J. Lewis, M. Raff, K. Roberts, and J. D. Watson, *Molecular Biology of the Cell*, 2nd ed., Garland Publishing, New York, 1989, p. 67.
7. J. L. Kroschwitz and M. Winokur, *Chemistry: General, Organic, Biological*, McGraw–Hill, New York, 1985, p. 634.
8. W. A. Bridger and J. F. Henderson, *Cell ATP*, Wiley-Interscience, New York, 1983, p. 1.
9. N. C. Price and L. Stevens, *Fundamentals of Enzymology*, 2nd ed., Oxford University Press, Oxford, UK, 1989, p. 5.
10. (a) *CSD Version 5.03*, Software Development Group, Crystallographic Data Centre, University Chemical Laboratory,

Cambridge, UK, 1992; (b) F. H. Allen, S. Bellard, M. D. Brice, B. A. Cartwright, A. Doubleday, H. Higgs, T. Hummelink, B. G. Hummelink–Peters, O. Kennard, W. D. S. Motherwell, J. R. Rodgers, and D. G. Watson, *Acta Cryst*., **B35**, 2331 (1979).

11. *GSTAT88 Version 5.1*, Software Development Group, Crystallographic Data Centre, University Chemical Laboratory, Cambridge, UK, 1992.
12. O. Ishitanl, S. Yanagida, S. Takamuku, and C. Pac, *J. Org. Chem*., **52**, 2790 (1987).
13. *MOLVIB* (in CHARMM, Version 22B), K. Kuzcera, J. Wiorkiewicz–Kuzcera, and M. Karplus, Dept. of Chemistry, Harvard University, 1987.
14. P. Pulay, G. Fogarasi, F. Pang, and J. E. Boggs, *J. Am. Chem. Soc*., **101**, 2550 (1979).
15. W. J. Hehre, L. Radom, P. Schleyer, and J. Pople, *Ab Initio Molecular Orbital Theory*, Wiley-Interscience, New York, 1986, p. 154.
16. W. E. Reilher, III, Ph.D. thesis, Harvard University, Cambridge, MA, 1985.
17. W. L. Jorgensen, *J. Phys. Chem*., **90**, 1276 (1986).
18. A. D. MacKerell, Jr. and M. Karplus, *J. Phys. Chem*., **91**, 10559 (1995).
19. W. L. Jorgensen, J. Chandrasekhar, J. D. Madura, R. W. Impey, and M. L. Klein, *J. Phys. Chem*., **79**, 926, (1979).
20. M. J. Field and M. Karplus, *CHARMM 22*, Dept. of Chemistry, Harvard University, 1988.
21. H. J. C. Berendsen, J. P. M. Postma, W. F. van Gunsteren, A. DiNola, and J. R. Haak, *J. Chem. Phys*., **81**, 3684 (1984).
22. J. P. Ryckaert, G. Ciccotti, and H. J. C. Berendsen, *J. Comput. Phys*. **23**, 327 (1977).
23. S. Ramaswamy, H. Eklund, and B. V. Plapp, *Biochemistry*, **33**, 5230 (1994).
24. C. L. Brooks, III and M. Karplus, *J. Mol. Biol*., **208**, 159 (1989).
25. M. J. Frisch, M. Head–Gordon, G. W. Trucks, J. B. Foresman, H. B. Schlegel, K. Raghavachari, M. A. Robb, J. S. Binkley, C. Gonzalez, D. J. Defrees, D. J. Fox, R. Whiteside, R. Seeger, C. F. Melius, J. Baker, R. L. Martin, L. R. Kahn, J. J. P. Stewart, S. Topiol, and J. A. Pople, *Gaussian 90*, Gaussian, Inc., Pittsburgh, PA, 1990.
26. Y. Wu and K. N. Houk, *J. Am. Chem. Soc*., **113**, 2353 (1991).
27. Y. Wu and K. N. Houk, *J. Org. Chem*., **58**, 2043 (1993).
28. B. S. Reddy, W. Saenger, K. Muhlegger, and G. Weimann, *J. Am. Chem. Soc*., **103**, 907, (1981).
29. K. Tu, D. J. Tobias, and J. Klein, *J. Phys. Chem*., **99**, 10035 (1995).
30. B. Roux and M. Karplus, *J. Comput. Chem*., **16**, 690 (1995).
31. R. H. Stote and M. Karplus, *Proteins*, **23**, 12 (1995).